Extreme events trigger turbulence decay: numerical verification of extreme value theory in pipe flows

Takahiro Nemoto [1,2] and Alexandros Alexakis[3]

[1]Philippe Meyer Institute for Theoretical Physics, Physics Department, École Normale Supérieure & PSL Research University, 24 rue Lhomond, 75231 Paris Cedex 05, France

[2]Mathematical Modelling of Infectious Diseases Unit, Institut Pasteur, 25-28 Rue du Docteur Roux, 75015 Paris, France

[3]Laboratoire de Physique Statistique, École Normale Supérieure, CNRS, Université Pierre et Marié Curie, Université Paris Diderot, 24 rue Lhomond, 75005 Paris Cedex 05, France

(Received xx; revised xx; accepted xx)

In pipe flow, turbulence locally created by a perturbation to laminar state shows sudden decay or splitting after a stochastic waiting time. A conjecture has been made that this sudden stochastic decay is triggered by extreme events, resulting in a fast (double-exponential) increase of the typical waiting time as the Reynolds number approaches its critical value. To investigate this conjecture, we perform, in parallel, more than 1000 pipe-flow direct numerical simulations (DNS) of the Navier-Stokes equations using a large number of computational resources, and measure the maximum value of axial vorticity field over the pipe (turbulence intensity). We show that the cumulative distribution function of this quantity is well approximated by Gumbel distribution function, confirming that the turbulence decay is described by the extreme value theory. Our observation provides the quantitative proof to the conjecture, and clarifies the mechanism of the fast (double exponential) increase of the turbulence decay's typical waiting time.

Key words: Turbulence, turbulent-Laminar transitions, pipe flows, extreme value statistics

1. Introduction

The laminar to turbulent transition in pipe flow is one of the most important problems in fluid mechanics (Eckhardt *et al.* 2007), initiated by O. Reynolds in 1887 (Reynolds 1883). The flow in a pipe is characterised by one non-dimensional parameter the Reynolds number, defined as $\mathrm{Re} = \mathrm{UR}/\nu$ where U is the flow velocity, R the diameter of the pipe, and ν the dynamic viscosity of the fluid. The question about the critical Reynolds number $\mathrm{Re_c}$ is simple: at which Reynolds number the flow in a pipe becomes turbulent from laminar (and *vice versa*). Though its apparent simpleness, answering this question was not straightforward due to a number of technical reasons (see (Eckhardt 2009) for a historical review of the critical Reynolds number). After 2000s, a localised turbulent state (Fig. 1) called "puff" (Wygnanski & Champagne 1973) created by a local perturbation to laminar flows has been studied in detail. The puff shows a sudden decay or splitting into two after a stochastic waiting time, which follows a memoryless exponential distribution (Hof *et al.* 2006, 2008; de Lozar & Hof 2009; Avila *et al.* 2010; Kuik *et al.* 2010). These

studies culminated in the estimation of the critical Reynolds number in 2011 (Avila *et al.* 2011), where Re_c was determined as Re at which the two typical times of the decay and splitting become equal. The obtained Re_c was about 2040 (Avila *et al.* 2011).

The critical Reynolds number was determined in laboratory experiments using long pipes. In direct numerical simulations (DNS) of the Navier-Stokes equation, the observation of critical Reynolds number has not yet been achieved because of too high computational costs. The current state of the art is to measure decay events up to $\mathrm{Re} = 1900$ and splitting events down to 2100 (Avila *et al.* 2011). There are several important benefits to measure these decay and splitting events in DNS. First, in experiments, unknown background noise that affects the results, could always exist. See, for example, (Eckhardt 2009) for a history of the struggle to determine the upper critical Reynolds number due to small background fluctuations. In DNS on the other hand, we know all the origin of the artificial noise, such as insufficient mesh sizes or periodic boundary effects, which can be easily controlled. Second, the quantities that can be measured in experiments are limited. For example, to determine the critical Reynolds number, a double-exponential fitting curve was heuristically used (Hof *et al.* 2006, 2008; Avila *et al.* 2011). The origin of this double-exponential law was argued using the extreme value theory (Goldenfeld *et al.* 2010; Goldenfeld & Shih 2017), where Goldenfeld *et al.* assumed a certain shape of the probability distribution function of maximum kinetic energy fluctuations. Mesurments of this probability function are out of reach in experiments, but can be achieved in DNS.

In this article by using high performance computing resources described in Acknowledgment, we study the statistics of turbulence decay in pipe flows. We perform more than 1000 independent single-core pipe-flow simulations in parallel (see Fig. 1) and determine the decay time up to $\mathrm{Re} = 2000$. Especially, we show that the cumulative distribution function of a maximal turbulence intensity (vorticity) is well described by the double-exponential Gumbel distribution. As a result, we verify the conjecture made by Goldenfeld *et al.* (Goldenfeld *et al.* 2010; Goldenfeld & Shih 2017) to explain the origin of the double-exponential empirical law for the turbulence decay time (Hof *et al.* 2006, 2008; Avila *et al.* 2011) in pipe flows.

2. Setup

We consider three dimensional pipe flows (with pipe length L and pipe diameter D) where the boundaries are periodic for z-axis and no-slip along the pipe (Fig. 1). The mean flow speed in z direction is denoted by U_b and we use the basic unit of length and time as D and D/U_b throughout this paper. The velocity field is denoted by $\boldsymbol{u}(\boldsymbol{r}, t)$ and we simulate it by solving the Navier-Stokes equation using an open source code (openpipeflow (Willis 2017)) whose validity has been vastly tested in many works (see Appendix A for the simulation detail). We simulate pipe flows for the Reynolds numbers below the critical value $\mathrm{Re} < \mathrm{Re}_\mathrm{c} \sim 2040$, where the flows tend to be laminar. We start the simulations with initial conditions where localised turbulence, *i.e.*, a turbulent puff, exists (see Appendix A for more details). If the Reynolds number is not too small (say, $\mathrm{Re} > 1850$), localised turbulent dynamics are sustained (Fig. 1). It quickly forgets their initial conditions and eventually decays after the stochastic time t, following an exponential distribution function (Hof *et al.* 2006, 2008; de Lozar & Hof 2009; Avila *et al.* 2010; Kuik *et al.* 2010): $p_\mathrm{d}(t) = (1/\tau_\mathrm{d}) \exp(-t/\tau_\mathrm{d})$, where τ_d is the typical decay time. This time scale τ_d is our target.

[t]

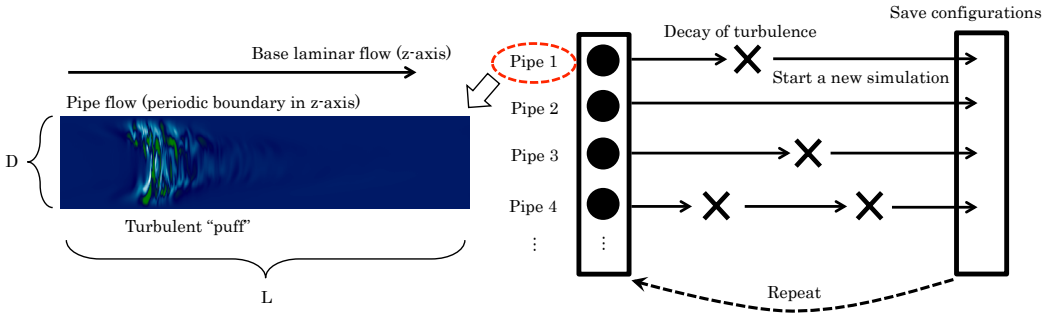

Figure 1: We simulate, in parallel, many single-core pipe flow simulations (from 96 to 1524 pipes at the same time), where each pipe has a diameter D and length L, and contains a single turbulent puff. We continue the simulations during a certain time interval (24 hours) and we store the configurations of velocity fields at the end of the simulations. Note that when a puff decays in a pipe, we immediately start another single puff simulation within that pipe. Using the final configurations as the next initial conditions, we repeat this procedure several times (from 10 to 40 times). We store the total simulation time T and the total number of decay events n_d for all pipes and for all repetitions, from which we estimate the typical decay time τ_d as detailed in the main text.

3. Results

3.1. *Measurements of* τ_d

To measure τ_d, we repeat many single-core pipe flow simulations in parallel and measure the total time T of all the simulations (ignoring initial relaxation times) and the number of decay events n_d that we observe during all the simulations (Fig. 1). Since the decay time is distributed exponentially (Hof *et al.* 2006, 2008; de Lozar & Hof 2009; Avila *et al.* 2010; Kuik *et al.* 2010), the probability of observing n_d decay events during a time interval T follows the poisson distribution

$$p_\mathrm{poisson}(n_\mathrm{d}) = \frac{e^{-T/\tau_\mathrm{d}}}{n_\mathrm{d}!}\left(\frac{T}{\tau_\mathrm{d}}\right)^{n_\mathrm{d}}. \tag{3.1}$$

As detailed in Appendix B, we then estimate τ_d and its error bars (95% confidence interval) from the observed data (n_d, T) by using Bayesian inference with an uninformative prior (which is a standard method to estimate Poisson event rate from observed data (Box & Tiao 2011)). This way of determining τ_d has the advantage that it accurately estimates error bars, which is important as we can only observe a few decay events when Reynolds number is large.

We show in Fig. 2 the obtained τ_d for different pipe lengths $L = 50D, L = 100D$ (red circles and blue squares, respectively) together with the experimentally fitted double exponential (yellow dashed) curve obtained in (Avila *et al.* 2011). For the Reynolds number up to 1900 (which has been studied so far using DNS), τ_d does not depend on the pipe length, and the results for both pipe lengths agree very well with the experimental data. However, as the Reynolds number increases, we observe that the results for $L = 100D$ deviate from those for $L = 50D$ and for the experiments. In DNS, periodic boundary conditions indicate that identical consecutive puffs are simulated, where the distance between these puffs is the pipe length L. An insufficient pipe length in DNS thus creates artificial correlations among the puffs, which play a role as noise to the dynamics and

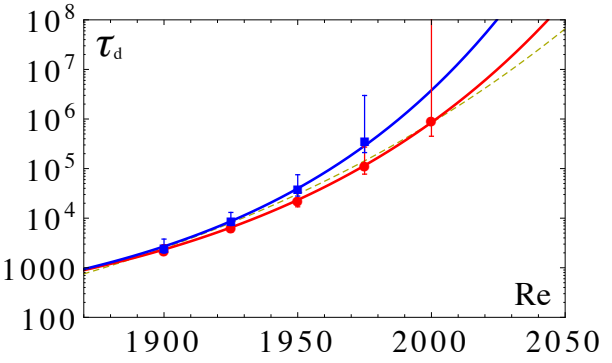

Figure 2: The typical decay time τ_d of turbulent puff in pipe flows obtained from DNS (red dots for $L = 50D$ and blue squared for $L = 100D$). Double exponential curves fitted to experiments (Avila *et al.* 2011) (yellow dashed line) and the theoretical lines (3.9) are also plotted as red and blue solid lines. In the theoretical lines, the parameters a, b are determined in Fig. 4(b), $\delta t = 1/4$, and $\Pi(h_x)$ is measured in Fig. 3(b). The error bars show 95% confidence interval (see Appendix B for the estimation of this confidence interval).

facilitate decay events. Note that the experimental results agree with the DNS result for $L = 50D$, even though the pipe lengths used for the experiments were much longer (Avila *et al.* 2011). Based on this observation, one could speculate that the experimental results were affected by small *unknown* background noise that facilitated the decay events, *i.e.*, the decay events close to critical Reynolds number could be ultrasensitive to tiny external perturbations. Further numerical and experimental studies are necessary to clarify this possibility. Below we discuss the derivation of the double-exponential formula for each *fixed* $L = 50D$ and $L = 100D$.

3.2. *Origin of the double-exponential formula*

To infer correctly the Reynolds number dependence of the time scale τ_d, a double-exponential fitting curve $\exp[\exp(\alpha \mathrm{Re} + \beta)]$ (with fitting parameters α, β) was used (Avila *et al.* 2011). Although this function can fit well to the experimentally observed time scale τ_d, the origin of this double exponential form is still conjectural. In the conjecture made by Goldenfeld *et al.* in 2010 (Goldenfeld *et al.* 2010), they assumed that the maximum of kinetic energy fluctuations over the pipe is distributed double exponentially (Gumbel distribution function) due to the extreme value theory (Fisher & Tippett 1928; Gumbel 1935). When this maximum goes below a certain threshold, turbulence decays. Assuming the linear dependence on Re of the parameters in the Gumbel distribution function, they thus derived the double-exponential increase of the time scale τ_d. Mathematically proving the validity of the extreme value theory and the linear scaling of the fitting parameters seems impossible, thus verifications in experiments or numerical simulations are needed. In laboratory experiments, the verification of this extreme value theory is not easy, as obtaining the maximum of a velocity field within a tiny turbulent puff is a non-trivial procedure. In this respect, numerical simulations have a strong advantage, because velocity fields are precisely tractable and the maximum of the fields is well-defined.

To this goal, we characterize the intensity of turbulence by the z-component of vorticity $H(\boldsymbol{r}, t) = (\nabla \times \boldsymbol{u})_z$. We then consider the maximum value of this turbulence intensity

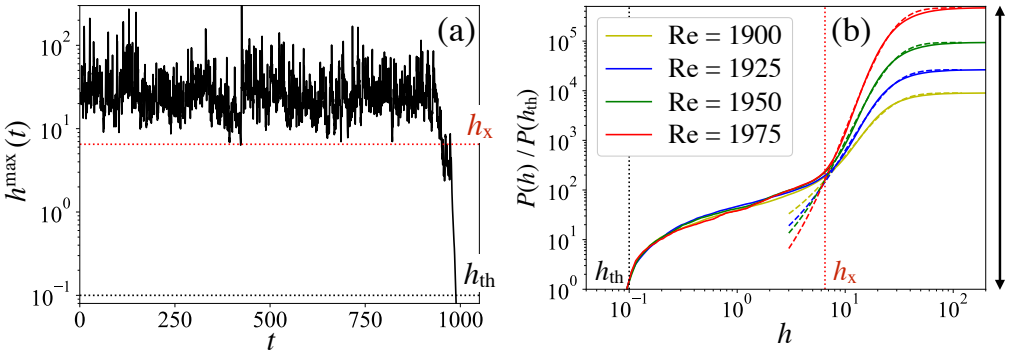

Figure 3: **(a)** An example of the maximum turbulence intensity $h^{\max}(t)$ for $L = 50D$ and $\mathrm{Re} = 1900$, where the puff decays when $t \simeq 1000$. We set $h_{\rm th} = 0.1$, shown as a black dotted line, throughout this paper, below which the maximum turbulence intensity always monotonically decreases (*i.e.*, puffs always decay). **(b)** The cumulative distribution of the maximum turbulence intensity $P(h)$ (3.3) divided by its minimum value $P(h_{\rm th})$, obtained from numerical simulations (solid coloured lines). The measurement interval δt is set to 1/4. The pipe length is set to $L = 50D$. (For $L = 100D$, similar results are obtained). Below a certain value $h_{\rm x}$, this function $P(h)/P(h_{\rm th})$ becomes independent of Reynolds number. This $h_{\rm x}$ is shown as a vertical red dotted line, and around 6.5 for $L = 50D$ and 7.5 for $L = 100D$. Above this value $h_{\rm x}$, $P(h)$ can be well approximated by the Gumbel function $P_{\rm Re}(h)$ (3.5). Dashed coloured lines are these Gumbel functions divided by $P(h_{\rm th})$. See Table 1 for the fitting parameters γ and h_0 used in this figure. Note that the value of $1/P(h_{\rm th})$ (for $\mathrm{Re} = 1975$) is the length of the double-headed arrow. From this figure, we estimate $\Pi(h_{\rm x}) \equiv P(h_{\rm x})/P(h_{\rm th}) \simeq 158.8$ for $L = 50D$ and 219.2 for $L = 100D$.

over the pipe

$$h^{\max}(t) = \max_{\boldsymbol{r}} H(\boldsymbol{r}, t). \tag{3.2}$$

Once this quantity goes below a certain threshold $h_{\rm th}$, $h^{\max}(t)$ monotonically decreases, leading to a quick decay of the puff (*i.e.*, the puff dynamics shows transient chaos (Barkley 2011; Hof *et al.* 2008)). See Fig. 3(a) for a decaying trajectory of $h^{\max}(t)$. In order to measure the cumulative distribution function of $h^{\max}(t)$ in our numerical simulations, we store $h^{\max}(t)$ for every fixed time interval δt. We denote by $(h^{\max}(t_i))_{i=1}^{N}$ the data obtained from all simulations with the number of measurements N. By using these data, we then define a cumulative distribution function $P(h)$ as the probability that $h^{\max}(t)$ takes a value less than or equal to h:

$$P(h) = \sum_{i=1}^{N} \frac{\Theta(h - h^{\max}(t_i))}{N} \tag{3.3}$$

with a Heaviside step function $\Theta(h)$. Note that the number of decay events $n_{\rm d}$ is written as $NP(h_{\rm th}) = \sum_{i=1}^{N} \Theta(h_{\rm th} - h^{\max}(t_i))$ by definition. This indicates that the decay time $\tau_{\rm d} \equiv (N\delta t)/n_{\rm d}$ is expressed as (Nemoto & Alexakis 2018)

$$\tau_{\rm d} = \frac{\delta t}{P(h_{\rm th})}, \tag{3.4}$$

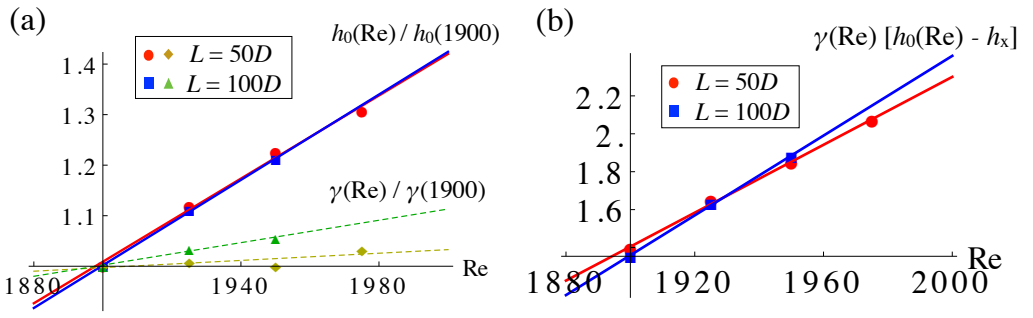

Figure 4: **(a)** The fitting parameters in the Gumbel function (3.5), γ and h_0, used in Fig. 3(b) (*i.e.*, the values summarised in Table 1) as a function of Re: Red circles (h_0 for $L = 50D$), yellow diamonds (γ for $L = 50D$), blue squares (h_0 for $L = 100D$), and green triangles (γ for $L = 100D$). To plot them together in the same panel, we divide each $\gamma(\mathrm{Re})$ and $h_0(\mathrm{Re})$ by $\gamma(1900)$ and $h_0(1900)$. They show linear dependence on Reynolds number: the solid and dashed straight lines are the linear fit. See Table 2 for the slopes and intercepts of these linear lines. Note that the slopes of the fitting lines for $h_0/h_0(1900)$ are much larger than those for $\gamma/\gamma(1900)$. **(b)** $\gamma(\mathrm{Re})[h_0(\mathrm{Re}) - h_\mathrm{x}]$ as a function of Re, where $\gamma(\mathrm{Re})$ and $h_0(\mathrm{Re})$ use the same values in the panel (a), and $h_\mathrm{x} = 6.5$ for $L = 50D$ and $h_\mathrm{x} = 7.5$ for $L = 100D$. We find a linear dependence: $\gamma(\mathrm{Re})[h_0(\mathrm{Re}) - h_\mathrm{x}] = a\ \mathrm{Re} + b$ (3.8). Here a and b are determined as $a = 0.00895442$, $b = -15.6087$ for $L = 50D$ and $a = 0.0105166$ and $b = -18.6222$ for $L = 100D$.

when N is sufficiently large. We set $h_\mathrm{th} = 0.1$ throughout this article †.

We measure this cumulative distribution $P(h)$ in DNS, rescale it by the threshold probability $P(h_\mathrm{th})$, and plot it in Fig 3(b). When h is smaller than a certain value h_x ($> h_\mathrm{th}$), the overlap in this scaled cumulative distribution is observed, *i.e.*, $P(h)/P(h_\mathrm{th}) \simeq \Pi(h)$ for $h < h_\mathrm{x}$ with a Re-independent function $\Pi(h)$. (Note that $h_\mathrm{x} \simeq 6.5$ for $L = 50D$ and $h_\mathrm{x} \simeq 7.5$ for $L = 100D$ from Fig 3(b)). When $h^\mathrm{max}(t)$ is smaller than h_x, dynamics are in a metastable state where the puff is hovering between death and life (see the panel (a) of Fig. 3). This overlap indicates that the dynamics in this metastable state are independent of (or less sensitive to) the change of the Reynolds number. Next, when h is greater than this value, we find that the $P(h)$ is well-described by a Gumbel distribution function P_Re:

$$P_\mathrm{Re}(h) \equiv \exp\left[-\exp\left(-\gamma(h - h_0)\right)\right], \tag{3.5}$$

where γ and h_0 are fitting parameters that depend on Re. In summary, we confirm that the scaled probability $P(h)/P(h_\mathrm{th})$ has the following form

$$\frac{P(h)}{P(h_\mathrm{th})} = \begin{cases} \Pi(h) & h \leqslant h_\mathrm{x} \\ P_\mathrm{Re}(h)/P(h_\mathrm{th}) & h > h_\mathrm{x}. \end{cases} \tag{3.6}$$

Based on the expression (3.5), the double-exponential increase of the turbulence decay time is justified as follows: From the continuity condition of (3.6) at $h = h_\mathrm{x}$, we get

† Precisely, the threshold value h_th should be defined as the value below which puffs always decay monotonically, but above which puffs have a certain probability to grow up and survive (even if this probability is very small). In reality, it is not easy to determine this precise value from numerical simulations. Fortunately, the magnitude of the errors (due to the inaccurate value of h_th) does not depend on the Reynolds number. When we consider Re close its critical value, these errors are therefore negligible because τ_d increases super-exponentially.

$\mathit{\Pi}(h_{\rm x}) = P_{\rm Re}(h_{\rm x})/P(h_{\rm th})$. Using the relation (3.4) that connects the decaying time $\tau_{\rm d}$ and $P(h_{\rm th})$, we then derive

$$\tau_{\rm d} = \delta t/P(h_{\rm th}) = \delta t\ \mathit{\Pi}(h_{\rm x})\ \exp\left[\exp\left(\gamma(h_0 - h_{\rm x})\right)\right]. \tag{3.7}$$

In the right-hand side of this expression, the Re-dependence only comes from γ and h_0, because $h_{\rm x}$ does not depend on Re (at least in the range of Re we are considering). In order to study Re-dependence on γ and h_0, we next plot these quantities as a function of Re in Fig. 4(a). The figure indicates that, within the examined range, these parameters depend linearly on Re. Especially, we can see that the slope of the linear fitting curve for γ is much smaller than that for h_0, which means we can approximate γh_0 as a linear function of Re. We thus get

$$\gamma(h_0 - h_{\rm x}) \simeq a\ {\rm Re} + b \tag{3.8}$$

with coefficients a and b. In Fig. 4(b), we confirm this linear approximation by plotting the left-hand side of (3.8) as a function of Re. We also determine the coefficients a and b from this figure, and summarise them in the caption of Fig. 4(b). Finally, using (3.8) in (3.7), we derive the double-exponential formula

$$\tau_{\rm d} \simeq \delta t\ \mathit{\Pi}(h_{\rm x}) \exp\left[\exp\left(a\ {\rm Re} + b\right)\right]. \tag{3.9}$$

Using $\delta t = 1/4$ and the values of $\mathit{\Pi}(h_{\rm x})$ measured in Fig. 3(b) (together with a, b obtained in Fig. 4(b)), we plot this double exponential formula in Fig. 2 as red and blue solid lines. The agreement between these theoretical lines with the direct measurements (red circles and blue squares) is excellent. Note that the parameters γ, h_0 are determined from the measurements up to Re $= 1975$ for $L = 50D$ and Re $= 1950$ for $L = 100D$. But the obtained curves agree with the direct measurements for Re $= 2000$ for $L = 50D$ and Re $= 1975$ for $L = 100D$. This observation indicates that our method can be used to infer statistical properties for higher Reynolds numbers from the data obtained in lower Reynolds numbers.

In our argument, the double exponential form in the decay time (3.9) comes from the Gumbel distribution function (3.5). The validity of this Gumbel description is where the extreme value theory could be relevant, e.g., one of the theorems used in the theory is Fisher-Tippett-Gnedenko theorem, which ensures that the cumulative distribution of the maximum value of a set of independent stochastic variables becomes the Gumbel distribution function (3.5) under some conditions (Fisher & Tippett 1928; Gumbel 1935). We do not expect that these conditions are *exactly* satisfied in our problem, because, for example, turbulent velocity fields are hardly independent from each other. Indeed, as shown in Fig. 5 of Appendix C, the deviations from the Gumbel distribution are clearly detected in the probability density (the derivative of the cumulative distribution in Fig. 3(b)). This discrepancy is contrasted to the recent observation done in (Shimizu *et al.* 2019) for channel flows. Anyway, as detailed above, our interest is $\tau_{\rm d}$ that is related to $1/P(h_{\rm th})$ (as indicated as the double-headed arrow in Fig 3(b)). This quantity is less affected by those deviations. Overall, the effect of the deviations on the decay time is small and can be neglected.

4. Conclusion

In this paper, using a large number of DNS, we measure the decay time of turbulent puff in pipe flows up to Re $= 2000$. In DNS, periodic boundary conditions are employed in the axial direction, so that the insufficient length of the pipe introduces artificial noise in puff dynamics. Our numerical simulations show that, as the length of the pipe increases

(*i.e.*, as this artificial noise decreases), the obtained decay times increase, resulting in values larger than those obtained in experiments (Avila *et al.* 2011) for large Reynolds numbers (that were not studied previously using DNS). This could indicate that the experimental results were affected by small (unknown) background noise that helped the turbulence to decay quickly. Further numerical and experimental studies are necessary to clarify this point.

To infer the decay time of puff, a double-exponential fitting curve has been heuristically used (Hof *et al.* 2006, 2008; Avila *et al.* 2011). It was conjectured in (Goldenfeld *et al.* 2010; Goldenfeld & Shih 2017) that this double-exponential form can be derived using the Gumbel distribution function of maximum kinetic energy fluctuations based on the extreme value theory. We measure the cumulative distribution function of the maximum turbulence intensity (3.2) and show that the function indeed approximately satisfies the Gumbel distribution function, proving that their conjecture is correct, in the range of the Reynolds numbers between 1900 and 2000.

As future perspectives, it is interesting to investigate, based on the extreme value theory, the universality of the argument to derive the double-exponential formula. For example, the same argument has been applied to turbulence decay problems in different geometries in (Shimizu *et al.* 2019). Furthermore, turbulent transitions between 2D- and 3D-dynamics have been long studied (Smith *et al.* 1996; Celani *et al.* 2010; Benavides & Alexakis 2017; Musacchio & Boffetta 2017; Alexakis & Biferale 2018), where a similar super exponential increase of the transition time was recently observed in thin-layer turbulent condensates (van Kan *et al.* 2019). This super-exponential increase could be also discussed based on the extreme value theory.

Studying these super exponential laws in DNS is computationally demanding. A brute-force approach using a large number of DNS is efficient as proven in this work. But exploiting so-called rare-event sampling methods could be also helpful. Such sampling methods include instanton methods based on Freidlin-Wentzell theory (Chernykh & Stepanov 2001; Heymann & Vanden-Eijnden 2008; Grafke *et al.* 2015*b*,*a*; Grigorio *et al.* 2017) as well as splitting methods to simulate several copies in parallel (Allen *et al.* 2005; Giardinà *et al.* 2006; Cérou & Guyader 2007; Tailleur & Kurchan 2007; Teo *et al.* 2016; Nemoto *et al.* 2016; Lestang *et al.* 2018; Bouchet *et al.* 2019). These methods have been successfully applied to many high dimensional chaotic dynamics.

Acknowledgements

The authors thank Dwight Barkley and Laurette Tuckerman for fruitful discussions and comments. This work was granted access to the HPC resources of CINES/TGCC under the allocation 2018-A0042A10457 made by GENCI (totally 3 million hours) and of MesoPSL financed by the Region Ile de France and the project Equip@Meso (reference ANR-10-EQPX-29-01) of the program Investissements d'Avenir supervised by the Agence Nationale pour la Recherche.

Appendix A. Simulation detail

We used an open source code openpipeflow (Willis 2017), which simulates flows in a cylindrical domain by solving the Navier-Stokes equation. Below are the summary of the parameters and settings we used:

• For azimuthal and longitudinal directions of the pipe, the spectral decomposition is used to evaluate the derivatives, for which we use 24 variables for azimuthal direction and 384 variables (for $L = 50D$) and 768 variables (for $L = 100D$) for longitudinal

directions. For the radial direction, finite-element method is used, for which the radial space is divided into 64 points using Chebyshev polynomials.

• The code can solve the Navier-Stokes equation under two conditions, fixed flux conditions and fixed pressure conditions. We especially use the fixed flux condition for the simulations.

• For the time step, the algorithm uses a second-order predictor-corrector scheme with automatic time-step control with courant number 0.5.

• We simulated totally 3 million hours to investigate the decay time following the way described in the main text (Fig. 1). We repeated in parallel many single-core pipe flow simulations (from $96 \sim 1524$ pipes) several times (from $10 \sim 40$ times), where each simulation lasts 24 hours.

• We defined that a puff decays when $h^{\max} < 0.1$ is satisfied. We never observed that a puff regenerates once $h^{\max} < 0.1$ is observed.

• To prepare initial velocity fields, we used a configuration where a single steady puff already exists. We added a small Gaussian noise to this configuration, and simulate during the time interval 50 or 100. These time intervals are our initial relaxation time. We checked that both initial relaxation times show consistent (almost the same) results for $\mathrm{Re} \geqslant 1900$. We set the measurement interval δt to be 1/4 (in units of D/U_{b}) for the simulations in Fig. 3(b).

Appendix B. Parameter inference for Poisson distribution

Here we summarise the method to infer the typical decay time τ_{d} from the observed decaying events.

Since the waiting time before observing a decaying event is distributed exponentially, the number n_{d} to observe multiple decaying events for a fixed time interval T follows the Poisson distribution

$$p_{\mathrm{poisson}}(n_{\mathrm{d}}) = \frac{e^{-\lambda_{\mathrm{d}} T}}{n_{\mathrm{d}}!} \left(\lambda_{\mathrm{d}} T\right)^{n_{\mathrm{d}}}, \tag{B 1}$$

where $\lambda_{\mathrm{d}} \equiv 1/\tau_{\mathrm{d}}$. Our aim is to estimate the parameter λ_{d} in this distribution from the number of decay events n_{d} observed in simulations. To this end, we use Bayes' rule, which allows us to construct a posterior probability distribution $p_{\mathrm{posterior}}(\lambda_{\mathrm{d}}|n_d)$, *i.e.*, the probability distribution of the parameter λ_{d} for a given observed data n_d, as follows:

$$P_{\mathrm{posterior}}(\lambda_{\mathrm{d}}|n_d) \propto p_{\mathrm{poisson}}(n_{\mathrm{d}}) Q_{\mathrm{prior}}(\lambda_{\mathrm{d}}). \tag{B 2}$$

Here $Q_{\mathrm{prior}}(\lambda_{\mathrm{d}})$ is a prior probability distribution that represents the initial guess of the parameter distribution. In our case, as we do not know the probability of λ_{d} *a priori*, we use a Jeffreys prior (an uninformative prior) defined as the square root of the determinant of the Fisher information (Box & Tiao 2011):

$$Q_{\mathrm{prior}}(\lambda_{\mathrm{d}}) \propto \frac{1}{\sqrt{\lambda_{\mathrm{d}}}}. \tag{B 3}$$

(Note that we checked that the results are not sensitive to the choice of prior probability distributions.)

The error bars are estimated using the posterior probability distribution $P_{\mathrm{posterior}}(\lambda_{\mathrm{d}}|n_d)$ as follows: first, we define 2.5%-quantile $\lambda_{\mathrm{d}}^{2.5}$ and 97.5%-quantile $\lambda_{\mathrm{d}}^{97.5}$ as the values of λ_{d} at which the cumulative posterior probability distribution takes 0.025 and 0.975,

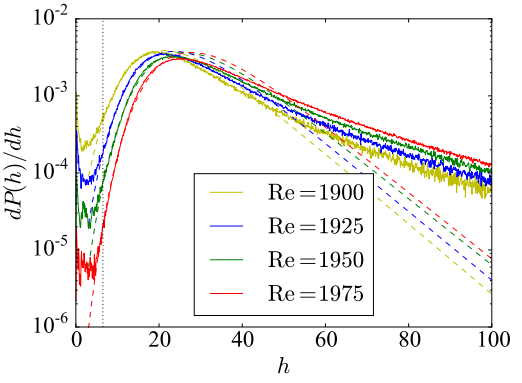

Figure 5: Probability distribution function of the maximum turbulence intensity $dP(h)/dh$ (where $P(h)$ is the cumulative distribution defined in (3.3)). The Gumbel probability distribution function, which is fitted to these curves, is also plotted in the same figure.

respectively:

$$\int_0^{\lambda_{\rm d}^{2.5}} d\lambda_{\rm d} P_{\rm posterior}(\lambda_{\rm d}|n_d) = 0.025, \tag{B 4}$$

$$\int_0^{\lambda_{\rm d}^{97.5}} d\lambda_{\rm d} P_{\rm posterior}(\lambda_{\rm d}|n_d) = 0.975. \tag{B 5}$$

Then 95% confidence interval is given as

$$\lambda_{\rm d}^{2.5} < \lambda_{\rm d} < \lambda_{\rm d}^{97.5}, \tag{B 6}$$

or

$$\frac{1}{\lambda_{\rm d}^{97.5}} < \tau_{\rm d} < \frac{1}{\lambda_{\rm d}^{2.5}}, \tag{B 7}$$

which is plotted as error bars in Fig.2.

Appendix C. Probability density of the turbulence intensity

From the cumulative distribution $P(h)$ of the maximum turbulence intensity (3.3), we define the corresponding probability density as its derivative $dP(h)/dh$. We calculate $dP(h)/dh$ from the data in Fig. 3(b) and plot it in Fig. 5 together with the corresponding Gumbel distribution $dP_{\rm Re}(h)/dh$ (where $P_{\rm Re}(h)$ is defined as (3.5)). We can see the discrepancies between the probability density and the Gumbel counterpart for $h > 20$ in Fig. 5. These discrepancies are hidden in the cumulative distributions as shown in Fig. 3(b), so that the argument to derive the super-exponentially increasing decaying time is intact.

REFERENCES

Alexakis, Alexandros & Biferale, Luca 2018 Cascades and transitions in turbulent flows. *Physics Reports* **767**, 1–101.

Allen, Rosalind J., Warren, Patrick B. & ten Wolde, Pieter Rein 2005 Sampling rare switching events in biochemical networks. *Phys. Rev. Lett.* **94**, 018104.

Table 1: Fitting parameters γ and h_0 for the Gumbel function (3.5) used in Fig. 3(b).

	Re = 1900	Re = 1925	Re = 1950	Re = 1975
$L = 50D$				
γ	0.0935183	0.0943595	0.0936482	0.0965271
h_0	21.401	23.9516	26.2484	27.9671
$L = 100D$				
γ	0.0891413	0.092231	0.0940843	-
h_0	22.6871	25.211	27.4782	-

Table 2: Fitting parameters determined in Fig. 4(a). $\bar{\gamma}(\mathrm{Re}) \equiv \gamma(\mathrm{Re})/\gamma(1900)$ and $\bar{h}_0(\mathrm{Re}) \equiv h_0(\mathrm{Re})/h_0(1900)$ are fitted with a linear function $S\ \mathrm{Re} + I$ with a slope S and an intercept I. See Table 1 for the values of $\gamma(1900), h_0(1900)$.

	Slope S	Intercept I
$L = 50D$		
$\bar{\gamma}$	0.000356	0.322
$\bar{h}_0$	0.00411	-6.80
$L = 100D$		
$\bar{\gamma}$	0.00111	-1.10
$\bar{h}_0$	0.00422	-7.02

Avila, Kerstin, Moxey, David, de Lozar, Alberto, Avila, Marc, Barkley, Dwight & Hof, Björn 2011 The onset of turbulence in pipe flow. *Science* **333** (6039), 192–196, arXiv: http://science.sciencemag.org/content/333/6039/192.full.pdf.

Avila, Marc, Willis, Ashley P & Hof, Björn 2010 On the transient nature of localized pipe flow turbulence. *Journal of Fluid Mechanics* **646**, 127–136.

Barkley, Dwight 2011 Simplifying the complexity of pipe flow. *Phys. Rev. E* **84**, 016309.

Benavides, Santiago Jose & Alexakis, Alexandros 2017 Critical transitions in thin layer turbulence. *Journal of Fluid Mechanics* **822**, 364–385.

Bouchet, Freddy, Rolland, Joran & Simonnet, Eric 2019 Rare event algorithm links transitions in turbulent flows with activated nucleations. *Phys. Rev. Lett.* **122**, 074502.

Box, George EP & Tiao, George C 2011 *Bayesian inference in statistical analysis*, , vol. 40. John Wiley & Sons.

Celani, Antonio, Musacchio, Stefano & Vincenzi, Dario 2010 Turbulence in more than two and less than three dimensions. *Phys. Rev. Lett.* **104**, 184506.

Cérou, Frédéric & Guyader, Arnaud 2007 Adaptive multilevel splitting for rare event analysis. *Stochastic Analysis and Applications* **25** (2), 417–443.

Chernykh, A. I. & Stepanov, M. G. 2001 Large negative velocity gradients in burgers turbulence. *Phys. Rev. E* **64**, 026306.

Eckhardt, Bruno 2009 Introduction. turbulence transition in pipe flow: 125th anniversary of the publication of reynolds' paper. *Philosophical Transactions of the Royal Society of London A: Mathematical, Physical and Engineering Sciences* **367** (1888), 449–455, arXiv: http://rsta.royalsocietypublishing.org/content/367/1888/449.full.pdf.

Eckhardt, Bruno, Schneider, Tobias M., Hof, Bjorn & Westerweel, Jerry 2007 Turbulence transition in pipe flow. *Annual Review of Fluid Mechanics* **39** (1), 447–468.

Fisher, Ronald Aylmer & Tippett, Leonard Henry Caleb 1928 Limiting forms of the frequency distribution of the largest or smallest member of a sample. In *Mathematical Proceedings of the Cambridge Philosophical Society*, , vol. 24, pp. 180–190. Cambridge University Press.

Giardinà, Cristian, Kurchan, Jorge & Peliti, Luca 2006 Direct evaluation of large-deviation functions. *Phys. Rev. Lett.* **96**, 120603.

Goldenfeld, Nigel, Guttenberg, Nicholas & Gioia, Gustavo 2010 Extreme fluctuations and the finite lifetime of the turbulent state. *Phys. Rev. E* **81**, 035304(R).

Goldenfeld, Nigel & Shih, Hong-Yan 2017 Turbulence as a problem in non-equilibrium statistical mechanics. *Journal of Statistical Physics* **167** (3), 575–594.

Grafke, Tobias, Grauer, Rainer & Schäfer, Tobias 2015*a* The instanton method and its numerical implementation in fluid mechanics. *Journal of Physics A: Mathematical and Theoretical* **48** (33), 333001.

Grafke, T., Grauer, R., Schäfer, T. & Vanden-Eijnden, E. 2015*b* Relevance of instantons in burgers turbulence. *EPL (Europhysics Letters)* **109** (3), 34003.

Grigorio, L S, Bouchet, F, Pereira, R M & Chevillard, L 2017 Instantons in a lagrangian model of turbulence. *Journal of Physics A: Mathematical and Theoretical* **50** (5), 055501.

Gumbel, Emil Julius 1935 Les valeurs extrêmes des distributions statistiques. *Ann. Inst. Henri Poincaré* **5** (2), 115–158.

Heymann, Matthias & Vanden-Eijnden, Eric 2008 Pathways of maximum likelihood for rare events in nonequilibrium systems: Application to nucleation in the presence of shear. *Phys. Rev. Lett.* **100**, 140601.

Hof, Björn, de Lozar, Alberto, Kuik, Dirk Jan & Westerweel, Jerry 2008 Repeller or attractor? selecting the dynamical model for the onset of turbulence in pipe flow. *Phys. Rev. Lett.* **101**, 214501.

Hof, Björn, Westerweel, Jerry, Schneider, Tobias M & Eckhardt, Bruno 2006 Finite lifetime of turbulence in shear flows. *Nature* **443** (7107), 59–62.

van Kan, Adrian, Nemoto, Takahiro & Alexakis, Alexandros 2019 Rare transitions to thin-layer turbulent condensates. *Journal of Fluid Mechanics* **878**, 356–369.

Kuik, Dirk Jan, Poelma, C. & Westerweel, Jerry 2010 Quantitative measurement of the lifetime of localized turbulence in pipe flow. *Journal of fluid mechanics* **645**, 529–539.

Lestang, Thibault, Ragone, Francesco, Bréhier, Charles-Edouard, Herbert, Corentin & Bouchet, Freddy 2018 Computing return times or return periods with rare event algorithms. *Journal of Statistical Mechanics: Theory and Experiment* **2018** (4), 043213.

de Lozar, Alberto & Hof, Björn 2009 An experimental study of the decay of turbulent puffs in pipe flow. *Philosophical Transactions of the Royal Society of London A: Mathematical, Physical and Engineering Sciences* **367** (1888), 589–599, arXiv: http://rsta.royalsocietypublishing.org/content/367/1888/589.full.pdf.

Musacchio, Stefano & Boffetta, Guido 2017 Split energy cascade in turbulent thin fluid layers. *Physics of Fluids* **29** (11), 111106.

Nemoto, Takahiro & Alexakis, Alexandros 2018 Method to measure efficiently rare fluctuations of turbulence intensity for turbulent-laminar transitions in pipe flows. *Phys. Rev. E* **97**, 022207.

Nemoto, Takahiro, Bouchet, Freddy, Jack, Robert L. & Lecomte, Vivien 2016 Population-dynamics method with a multicanonical feedback control. *Phys. Rev. E* **93**, 062123.

Reynolds, Osborne 1883 An experimental investigation of the circumstances which determine whether the motion of water shall be direct or sinuous, and of the law of resistance in parallel channels. *Proceedings of the royal society of London* **35** (224–226), 84–99.

Shimizu, Masaki, Kanazawa, Takahiro & Kawahara, Genta 2019 Exponential growth of lifetime of localized turbulence with its extent in channel flow. *Fluid Dynamics Research* **51** (1), 011404.

Smith, Leslie M, Chasnov, Jeffrey R & Waleffe, Fabian 1996 Crossover from two-to three-dimensional turbulence. *Physical review letters* **77** (12), 2467.

Tailleur, Julien & Kurchan, Jorge 2007 Probing rare physical trajectories with lyapunov weighted dynamics. *Nature Physics* **3** (3), 203.

Teo, Ivan, Mayne, Christopher G., Schulten, Klaus & Lelièvre, Tony 2016 Adaptive multilevel splitting method for molecular dynamics calculation of benzamidine-trypsin dissociation time. *Journal of Chemical Theory and Computation* **12** (6), 2983–2989, pMID: 27159059.

Willis, Ashley P. 2017 The openpipeflow navier-stokes solver. *SoftwareX* **6**, 124 – 127.

Wygnanski, I. J. & Champagne, F. H. 1973 On transition in a pipe. part 1. the origin of puffs and slugs and the flow in a turbulent slug. *Journal of Fluid Mechanics* **59** (02), 281–335.